Available online at www.sciencedirect.com
SCIENCE DIRECT
Polymer 45 (2004) 8265–8277
polymer
www.elsevier.com/locate/polymer

Crystallographic texture, amorphization, and recrystallization in rolled and heat treated polyethylene terephthalate (PET)

D. Raabe[a,*], N. Chen[b], L. Chen[c]

[a]*Department of Microstructure Physics, Max-Planck-Institut für Eisenforschung, Max-Planck-Str. 1, 40237 Düsseldorf, Germany*
[b]*Engineering Division, Colorado School of Mines, Golden, CO 80401, USA*
[c]*School of Material Science and Engineering, University of Science and Technology, Beijing, China*

Received 4 January 2004; received in revised form 25 August 2004; accepted 17 September 2004
Available online 12 October 2004

Abstract

This study is about crystallographic texture, deformation-induced decrystallization (disaggregation, amorphization), and subsequent recrystallization in rolled and heat treated semi-crystalline (triclinic) PET. Experiments are based on quantitative wide angle X-ray diffraction using an area detector. The change in crystallinity during rolling deformation and heating is analyzed in terms of X-ray data (peaks and background) that are integrated over the entire pole sphere. This method eliminates texture effects in the analysis of crystallinity. The rolling texture consists of a $\{100\}\langle 001\rangle$ component and an incomplete fiber ($\langle 001\rangle \| $rolling direction). The texture is explained by crystallographic shear mainly on $\{100\}\langle 001\rangle$ intralamellar shear systems. The X-ray analysis reveals that crystallinity drastically decreases during rolling. We suggest that amorphization (disaggregation, decrystallization) is a deformation mechanism which takes place as an alternative to crystallographic intralamellar shear depending on the orientation of the lamellae. Heat treatment (373, 473 K) leads to the recrystallization of amorphous material and to an enhancement of the original deformation texture. We explain the recrystallization texture in terms of an oriented nucleation mechanism where amorphous material aligns along existing crystalline lamellae.

Keywords: Texture; X-ray diffraction; Polymer

1. Introduction

Polyethylene terephthalate (PET) is widely used for manufacturing packaging devices, electrical components, as well as film and recording tapes. The mechanical and functional properties of PET depend on the degree of crystallinity and on the crystallographic orientation distribution (texture). Both microstructure parameters evolve in a characteristic way during mechanical loading and thermal treatment.

A number of thorough investigations has been published on the crystallographic textures of PET, particularly on those evolving during large-strain plastic deformation. However, some questions associated with the underlying mechanisms of texture formation during deformation, strain-induced loss of crystallinity (disaggregation, solid-state amorphization), and temperature-induced increase in crystallinity (recrystallization of amorphous material) in PET are still unresolved. This statement requires some explanation.

First, previous approaches to these topics were not based on *quantitative* texture data since they used $\theta-2\theta$ wide angle X-ray diffraction scans or two-dimensional pole figure data. For instance, Llana and Boyce [1] studied polymer textures under uniaxial and plane strain compression using $\theta-2\theta$ scans. Such scans are not quantitative and provide reliable data only in the cases of totally random or strong fiber textures. Recently the use of area detectors in conjunction with wide angle X-ray scattering has received increasing attention due to their capability to acquire Debye–Scherrer images which provide more structural information than conventional point scintillation counters. For instance Asano et al. [2] investigated the crystallization behavior of deformed amorphous PET films after different

* Corresponding author. Tel.: +49 211 6792278; fax: +49 211 6792333.
E-mail address: raabe@mpie.de (D. Raabe).

0032-3861/$ - see front matter © 2004 Published by Elsevier Ltd.
doi:10.1016/j.polymer.2004.09.045

annealing times using X-ray diffraction and microhardness. In a related study Asano et al. [3] also measured the melting behavior of textured polypropylene which was crystallized by the temperature slope method. Mahendrasingama et al. [4] investigated the influence of temperature and chain orientation on the crystallization behavior of PET during drawing. Bedia et al. [5] investigated the texture evolution of polyethylene naphthalate/polyethylene terephthalate blends under uniaxial drawing. Bellare et al. [6] conducted a very detailed study on the development of crystallographic texture in PET deformed by plane–strain compression. Similar studies on polymer textures are in Refs. [7–9].

While these works provide fundamental insight with respect to some of the points mentioned above, a more detailed study on the evolution of crystallographic texture and crystallinity in polymers requires pole figure inversion, i.e. the use of the orientation distribution function (ODF) [10,11]. The current work presents for the first time such a quantitative and systematic approach to the joint investigation of texture and crystallinity of rolled and heat treated PET. Our study is based on the measurement of wide angle X-ray Debye–Scherrer images by an area detector. We use these data for quantitative texture analysis and for the investigation of the transition between the amorphous and the crystalline state in PET during rolling deformation and heat treatment. In contrast to standard procedures for texture analysis known from metals and ceramics the investigation of PET textures is more challenging. This is due to the fact that it has triclinic crystal structure, contains amorphous and crystalline portions, and reveals pronounced Bragg-peak broadening during deformation owing to the strain- and heat dependent transition between the two phases.

The second basic problem associated with the quantitative investigation of texture and crystallinity of semi-crystalline polymers arises from the complicated microstructure of these materials. They consist of spherulites that contain nanoscaled crystalline lamellae embedded in an amorphous matrix. The lamellae are typically heavily branched so that each spherulite in itself is not single but polycrystalline. Further rotational degrees of freedom can add to this spherulite texture due to the molecular conformation of the constituent monomers and the resulting helix angle of the crystalline chains [12,13]. This complexity of the microstructure means that the *local* micromechanical boundary conditions controlling the reorientation of polymer crystals during straining are not well known.

For example different microscopic mechanisms are conceivable for a crystal to rotate during deformation. One possibility is that crystals rotate due to the elastic–plastic spin arising from their internal crystallographic shear, i.e. from their intralamellar slipping systems (active orientation change). Another possibility is that crystals may rotate due to skew-symmetric boundary conditions exerted as a consequence of gradients in the compliance of their amorphous neighborhood (passive orientation change). In other words both, the crystalline reorientation mechanisms and the local boundary conditions during mechanical loading are not well known. This makes it difficult to model orientation changes in semi-crystalline polymers in terms of conventional micromechanical texture models so that more complex formulations must be developed [14–17].

A third issue in the context of texture and structural stability of semi-crystalline polymers are the mechanisms of strain-induced amorphization on the one hand and thermally-induced recrystallization of amorphous material on the other hand. Both processes establish a close kinetic link between the two thermodynamic states and their micromechanical behavior. This means also that crystallographic texture and crystallinity are related problems. Earlier work of Chaari et al. [18] showed that above and close to T_g, the crystallization kinetics in PET can be promoted by preceding deformation. The authors also found that the decrease of crystallinity was dependent on the deformation rate, on the temperature, and on the total plastic strain. It was also observed that a certain pre-strain level promotes further crystallization of bulk amorphous PET even after the deformation has ceased as shown by Chaari et al. [18], Gorlier et al. [19], and Zhang et al. [20]. Owing to these earlier findings we believe that quantitative texture analysis in conjunction with the determination of the change in crystallinity can help to identify the orientation dependence of both mechanisms. As far as amorphization is concerned it is likely that crystals which have an unfavorable orientation for intralamellar crystallographic shear[1] (Schmid factor equal to zero) may instead undergo structural disintegration, i.e. amorphization as an orientation-dependent mode of deformation. Different mechanisms are conceivable to govern the details of such a process (see chapter 4).

Also, the formation of recrystallization textures is not well understood in such matter. While it is known that the material that was rendered amorphous during deformation can subsequently recrystallize (relax) upon sufficient heat treatment it is unclear from the literature whether this process follows an oriented nucleation or growth selection mechanisms. It is likely that joint texture and crystallinity measurements can elucidate this point.

Therefore, as far as methodology is concerned, the goal of this study lies in applying for the first time pole figure inversion by means of the texture component method to the quantitative investigation of polymer textures. This approach works in quaternion space and reproduces sets of discrete 3D spherical Gaussian texture components together with their intensity and orientational scatter width from corresponding 2D diffraction data [21,22]. In that

[1] It must be underlined in this context that crystallographic shear does not necessarily require dislocation motion in PET. Crystallographic slip may in many crystalline polymers occur in the form of simple rigid shears on van der Waals bonded (soft) planes in the crystals or by the rigid intralamellar shear between more compact small crystalline blocks within the same lamellae.

context we also aim to exploit specific properties of the area detector for background investigation in terms of the integration and analysis of complete sets of Debye–Scherrer frames.

As far as microstructure is concerned the aim of this investigation is the quantitative measurement and qualitative understanding of the basic mechanisms which govern the formation of crystallographic textures in PET during rolling in terms of crystallographic shear and strain-induced amorphization as well as during recrystallization in terms of crystal nucleation and growth in amorphous material.

2. Experimental

2.1. Sample material and processing

The study was conducted on commercial semi-crystalline PET. The weight-average molecular weight (M_W) of the PET amounted to 25,000 g/mol. The polydispersity was about 2.0. The material contained small amounts of antimony and phosphate, but no plasticizer were used. The starting sheet material was in a partially crystalline state (crystalline volume fraction of about 85% in the undeformed state) and had a nearly random crystallographic texture. The density before the rolling deformation amounted to 1.33 g cm^{-3}. The glass transition temperature of the material is 354 K and its melting point 528 K. Both quantities refer to the undeformed state.

The mechanical experiments were started with PET sheets of an initial thickness of 10 mm. The samples were rolled at room temperature. Each pass exerted a thickness reduction of about 0.1 mm. Crystallographic textures were measured on samples deformed to different true (logarithmic) strain levels. Samples with a true strain of 1.2 were heat treated at 373 and 473 K, respectively, for different annealing times ranging from 2 s to 160 min.

2.2. Measurement of Debye–Scherrer diagrams and pole figure calculation

The texture measurements were carried out on an X-ray texture goniometer in the back-reflection mode. The instrument was equipped with an area detector for the direct electronic imaging of X-ray Debye–Scherrer patterns. The measurements were carried out using Cr $K_{\alpha 1}$ radiation at a tube current of 40 mA and a voltage of 40 kV. The distance between sample and area detector was 158 mm. For reconstructing complete Debye–Scherrer diagrams covering the entire pole sphere we collected 162 frames for each sample condition. The integration time for each single frame amounted to 100 s in order to capture sufficient intensity. All diffraction data were normalized and corrected for geometrical effects. From the normalized and corrected Debye–Scherrer measurements {100}, {1$\bar{1}$0}, and {010} pole figures were reconstructed. The sample symmetry was orthorhombic (owing to the symmetry imposed by the rolling process) and the crystal symmetry triclinic. The parameters of the unit cell are $a=4.5$ Å, $b=5.9$ Å, $c=107$ Å, $\alpha=100°$, $\beta=118°$, and $\gamma=112°$ [23].

2.3. Approaches to the quantitative analysis of PET textures

2.3.1. Basics of quantitative texture analysis for polymers

Pole figures serve as input for the calculation of the ODF. For this purpose different approaches can be used, namely, the so called direct pole figure inversion methods, the Fourier-based series expansion methods which use spherical harmonics as library functions, and the texture component method which reproduces the orientation distribution in terms of sets of preferred orientations with *individual* spherical scatter and amplitude. Overviews on the different approaches were given by Bunge [10] and Raabe [11].

In this study we have chosen the texture component method in the formulation of Helming et al. [22] for quantitative texture analysis. The method works in quaternion space and uses sets of Gauss or Lorentz-shaped spherical model functions with individual height and individual full width at half maximum as a measure for the strength and spherical scatter of a crystallographic texture component. The ODF is approximated by a linear superposition of such functions as outlined in detail in the next section.

2.3.2. Quantitative texture analysis by use of the texture component method

According to Lücke et al. [21] and Helming et al. [22] the mathematical reproduction of the ODF by texture component functions can be expressed by the superposition

$$f(g) = F + \sum_{c=1}^{C} I^c f^c(g) = \sum_{c=0}^{C} I^c f^c(g) \quad \text{where } I^0 = F,\ f^0(g) = 1 \tag{1}$$

where g is the orientation, $f(g)$ is the ODF and F is the volume portion of all randomly oriented crystals (random texture component). F may be understood as the intensity of the only *global* component used in the approximation, equivalent to for each orientation point in Euler space, $g \in G$. The intensity I^c describes the volume fraction of all crystals belonging to the texture component c. It must be underlined at this point that a texture component does not represent a single crystalline lamella in the PET sample but a set of crystalline material portions, which can be summarized in the form of a common isotropic spherical distribution function. This means that a spherical texture component c is described in terms of a maximum orientation density at a preferred orientation g^c and scatter width b^c [22]. The orientation density of the component is represented by a function the value of which decreases in an isotropic fashion with increasing orientation distance

$\tilde{\omega}^c = \tilde{\omega}(g^c, g)$ from the maximum. This means that $f^c(g)$ only depends on $\tilde{\omega}^c = \tilde{\omega}(g^c, g)$ and is independent on the rotation axis $\tilde{n}^c$. The ODF is defined by

$$f(g)\mathrm{d}g = 8\pi^2 \frac{\mathrm{d}V_g}{V} \quad \text{which implies } f(g) \geq 0 \tag{2}$$

where V is the sample volume and $\mathrm{d}V_g$ the volume of all crystals with an orientation g within the orientation portion $\mathrm{d}g = \sin(\phi)\,\mathrm{d}\phi\,\mathrm{d}\phi_1\,\mathrm{d}\phi_2$. Normalization requires

$$\oint f^c(g)\mathrm{d}g = 1 \quad \text{which implies } \sum_{c=0}^{C} I^c = 1 \tag{3}$$

As a rule texture components require positivity, i.e.

$$f^c(g) \geq 0 \quad \text{for all } g \in G \text{ and } I^c > 0 \tag{4}$$

where G is the orientation space.

Distribution functions which have a maximum at a preferred orientation g^c and decrease with increasing orientation distance $\tilde{\omega}^c = \tilde{\omega}(g^c, g)$ are referred to as central functions. Such functions, including corresponding pole figures, can be represented in the form of series expansions of χ functions or respectively Legendre polynomials. More practical approximations of texture components can be obtained by using spherical standard functions. The examples presented later in this work make use of Gauss-shaped model functions for the de-composition of the orientation distribution function which are described by

$$f^c(g) = N^c \exp(S^c \cos\tilde{\omega}) \tag{5}$$

where

$$S^c = \frac{\ln 2}{1 - \cos(c^c/2)} \quad \text{and} \quad N^c = \frac{1}{I_0(S^c) - I_1(S^c)} \tag{6}$$

The corresponding pole figure projections $P_h^M(g^c, b^c, y)$ can be calculated in analytical form

$$P_h^M(g^c, b^c, y) = N^c \exp(S^c \sin(\upsilon^c/2)) I_0(S^c \cos(\upsilon^c/2)) \tag{7}$$

where υ^c describes the geometry of the component in the respective pole figure projection and $I_l(x)$ are generalized Bessel functions. The value b^c is the halfwidth and can be interpreted as the mean diameter of a spherical component in orientation space [22]. The components describing $f(g)$ can be determined by the best fit of the experimental pole figure input data $\tilde{P}_{h_i}^M(y_r)/N_{h_i}$ with the recalculated pole figures $\sum_c I^c \tilde{P}_h^M(g^c, b^c, y_r)$. The index r marks the measured sample directions y_r. The component parameters I^c, g^c and b^c and the normalization N_{h_i} of the pole figures are obtained by solving the least squares problem

$$\sum_{i,r} w_{ir} \left[\tilde{P}_{h_i}(y_r)/N_{h_i} - \sum_c I^c \tilde{P}_{h_i}^M(g^c, b^c, y_r) \right]^2 \Rightarrow \mathrm{Min}. \tag{8}$$

where w_{ir} are weight factors. Usually the parameters g^c and b^c must be calculated by a non-linear algorithm. First estimates are required, which may be obtained manually from the graphical representation of the difference pole figures which are calculated according to

$$\Delta_{h_i}(y_r) = \tilde{P}_{h_i}(y_r) - \sum_c I^c \tilde{P}_{h_i}^M(g^c, b^c, y_r) \tag{9}$$

Depending on experience in interpreting crystallographic textures the user can specify the position, height, and scatter of the texture components within certain bounds before the minimization. This makes particularly sense, when the number of texture components initially prescribed to match an experimental texture is small or when a certain scatter width of the components should not be exceeded. Further details on the method are given in the works of Lücke et al. [21] and Helming et al. [22]. The texture component version used for this study is the one described by Helming.

3. Experimental results

3.1. Evolution of crystallographic texture during rolling

Fig. 1 shows the texture evolution during room temperature rolling in terms of three different pole figure projections. The pole figures are corrected for background and normalized. The initial texture of the material before deformation was practically random. At a true (logarithmic) rolling strain of 0.5 a weak texture has formed with a maximum pole density below 1.5. At a strain of 0.9 the texture has become more pronounced. It is characterized by an orientation fiber with the rolling direction as a common rotation axis. The normal direction (compression plane during rolling) is characterized by a pronounced {100} pole density. At a larger true strain of 1.2 the fiber texture has sharpened.

Fig. 2 exemplary shows a texture component fit for a sample rolled to a true strain of 1.2. By using the texture component method introduced above the crystallographic texture was decomposed into two main texture components, namely, one texture component close to $\{100\}\langle 001\rangle$ and a fiber texture component $\langle 001\rangle \| \mathrm{RD}$ (triclinic RD fiber component)[2] where RD refers to the rolling direction.

In order to avoid misinterpretations it must be underlined at this point that the texture fit is quantitative, i.e. it is conducted in quaternion space and not in the projected pole figure space. The presentation of the recalculated pole figures serves only as a qualitative check of the match between the original corrected and normalized raw data and the approximated texture obtained from the fitting

[2] The Miller notation for the triclinic component, $\{001\}\langle 001\rangle$, indicates that the component is characterized by a crystallographic {100} plane parallel to the normal (compression) plane and a $\langle 001\rangle$ direction parallel to the rolling direction. Since the crystal structure of PET is triclinic the indices {100} represent the (100) and the $(\bar{1}00)$ planes, but not the (010), $(0\bar{1}0)$, (001), or $(00\bar{1})$ planes. The indices for $\langle 001\rangle$ direction represent the [001] and the $[00\bar{1}]$ directions, but not the [010], $[0\bar{1}0]$, [100], or $[\bar{1}00]$.

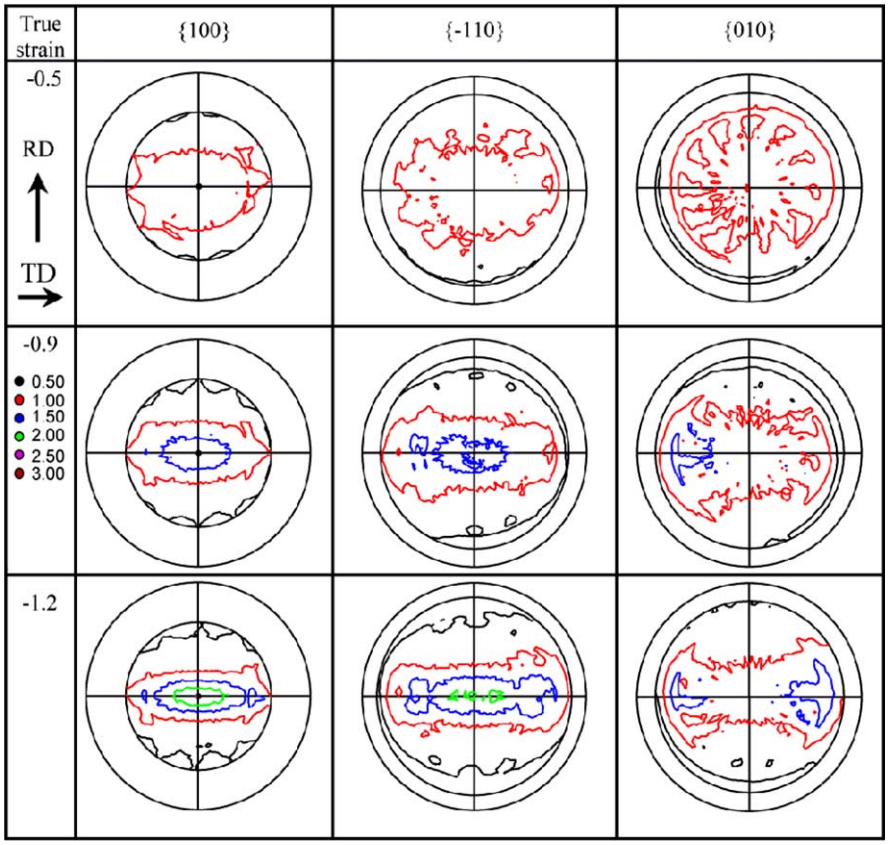

Fig. 1. Experimental pole figures obtained from Debye–Scherrer images for rolled PET (triclinic crystal structure). Rolling was carried out at room temperature. The texture before rolling was nearly random.

procedure. The numerical fitting procedure allows the user to start with several possible texture components. As outlined in the preceding chapter a minimization routine automatically calculates the component distribution (i.e. the volume fraction and the half width of the orientation components) in 3D orientation space using Bessel-normalized Gaussians or Lorentz functions.

Fig. 3 gives an overview of the evolution of the texture in

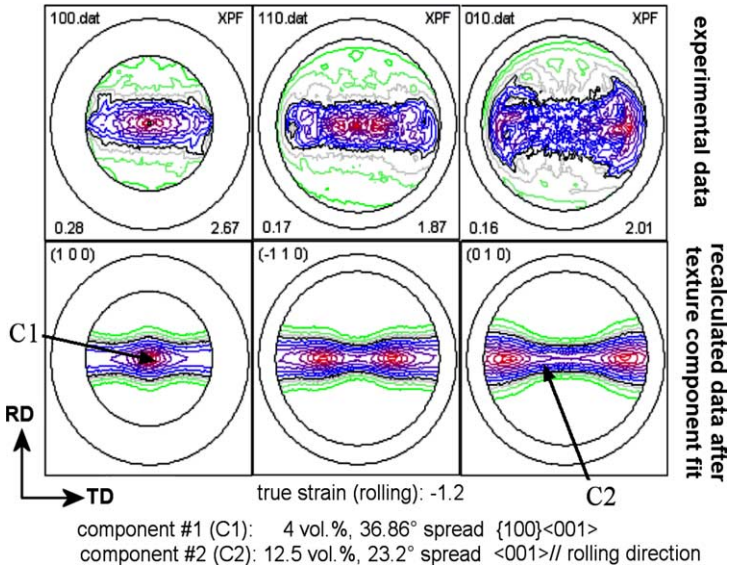

Fig. 2. Example of the texture component fit from experimental pole figures on the basis of the approach of Helming et al. [22] using spherical Gauss functions. The upper row shows the experimental data. The lower row shows the recalculated pole figures after the component fit. The texture consists of two main texture components, namely, a $\{100\}\langle001\rangle$ component (triclinic component with a strong $\{100\}$ plane parallel to the surface and a fiber component $\langle001\rangle\|$RD (triclinic RD fiber component). The true rolling strain amounts to 1.2.

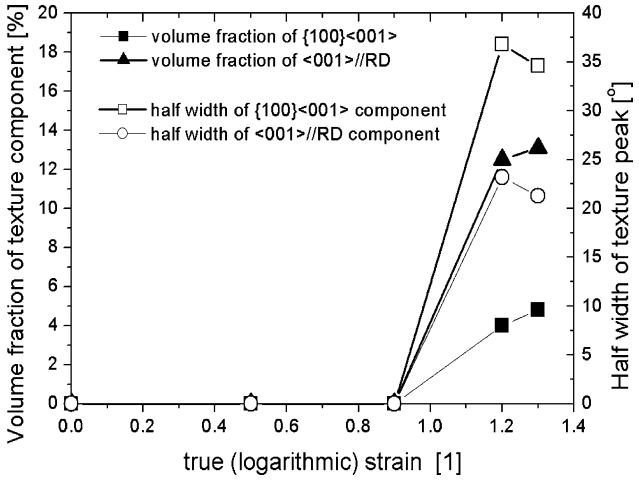

Fig. 3. Development of the crystallographic texture in terms of the volume fractions and spherical half widths of the two main orientation components during rolling. The data were calculated by use of the texture component method from the pole figures shown in Fig. 1. The volume fraction of both components increases, i.e. the texture becomes more pronounced during room temperature rolling.

terms of the volume fractions and half widths of the two main orientation components during rolling. The data were calculated by use of the texture component method from the pole figure shown in Fig. 1. The diagram shows that the volume fractions and the half widths of both components increase with increasing rolling strain. At true strains above 1.2 the spherical half widths become smaller which indicates an increase in texture sharpness (less orientation scatter of the texture components). For instance, the triclinic component (Gauss standard function), $\{100\}\langle 001\rangle$, occupies a volume fraction of 4% at a full width at half maximum of 36.96° after a strain of 1.2. The triclinic RD fiber component occupies a volume fraction of 12.5% at a full width at half maximum of 23.2°.

3.2. Evolution of crystallinity during rolling

The measurement of the change in crystallinity of PET during rolling is based on the complete integration of the background and Bragg-peak data over the entire pole sphere in terms of 162 separate Debye–Scherrer frames using an integration time of 100 s for each frame.

Fig. 4 shows two Debye–Scherrer frames which were taken at two different tilting angles, $\phi = 0°$ and $\phi = 90°$. The difference of the patterns demonstrates how strongly diffraction data may depend on the position of the measurement on the pole sphere. This observation underlines that the measurement of the degree of crystallinity of polymers cannot be made by simple $\theta - 2\theta$ X-ray wide angle line scans but requires instead to take the crystallographic texture of the material properly into account.

It must be noted in this context that the number of X-ray counts determined for the diffuse background scatter should in principle be independent on the orientation of the

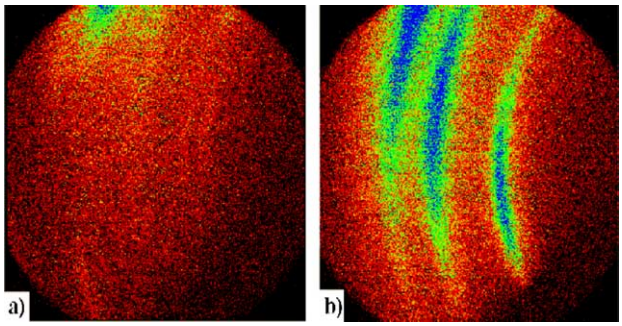

Fig. 4. Debye–Scherrer frames taken for two different tilting angles, ϕ. The different patterns reveal qualitatively how strongly the diffraction data depend on the position of the measurement on the pole sphere. This means that the measurement of the degree of crystallinity cannot be made by simple $\theta - 2\theta$ X-ray wide angle line scans. Such analysis must in principle take texture into account. (a) $\phi = 0°$ (b) $\phi = 90°$.

measurement. However, the pronounced broadening of the Bragg cones, which seems to be typical of the gradual structural changes in the PET during deformation, produces an uneven distribution of the out-of-reflex X-ray scatter. In particular the gradual broadening of the Bragg cones is much more pronounced for rolled PET (and also for other partially-crystalline polymers) than for metals and makes it sometimes difficult to clearly differentiate between Bragg diffraction and diffuse wide angle scatter. Therefore, in order to obtain quantitative data all measured frames for one sample condition were summed up into one single Debye–Scherrer frame. This averaged Debye–Scherrer frame was then integrated into a single wide angle X-ray $\theta - 2\theta$ scan which represents a complete integration of the Bragg- and out-of-Bragg density distribution of the X-ray scatter over the entire pole sphere.

Fig. 5a shows the integrated wide angle X-ray scans as a function of the accumulated rolling strain. The figure reveals that the curves become gradually smoother during rolling, i.e. the Bragg peaks are less pronounced relative to the background level at large strains. The Bragg cones occurring in the undeformed PET sheets ($\phi = 0$, black squares) are becoming broader as a function of deformation (compare to $\phi = 1.3$, open squares). This corresponds to a drop in the crystalline volume fraction. It must be underscored that this degradation in Bragg scatter relative to the background scatter is not due to a change in texture since the data are averaged over the entire pole sphere comprising the signals of crystals of *all* possible orientations. This means that texture effects are eliminated in the integration.

Fig. 5b shows the integrated number of counts, the integrated number of background counts, and the relative change in the normalized number of all counts minus the background counts as a function of deformation. The latter curve (open squares in the diagram) shows the relative change in crystallinity. The strong increase in the diffuse background when compared to all counts indicates a relative

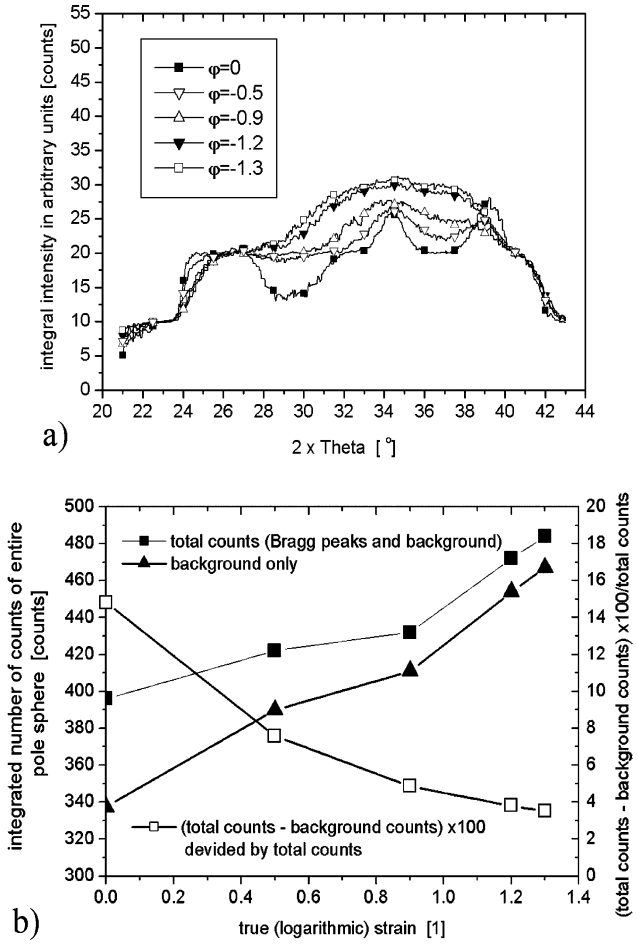

Fig. 5. (a) Integrated wide angle X-ray scans ($\theta-2\theta$ scans) as a function of rolling strain. Integration is conducted over all Debye–Scherrer frames measured for one sample condition. (b) Integrated number of total counts (full squares), integrated number of background counts (full triangles), and change (in %) in the normalized number of all counts minus the background counts as a function of deformation. The latter curve (open squares) shows the change in crystallinity during rolling.

drop in crystallinity with increasing total strain from ~15% to ~3% (in arbitrary units).

3.3. Evolution of the crystallographic texture during heat treatment

Fig. 6 shows the texture evolution of rolled PET (true strain $\phi=1.2$, rolled at room temperature) during a subsequent heat treatment at 373 and 473 K, respectively, in terms of pole figures. The data show that the initial deformation texture becomes stronger during annealing (compare to Fig. 1, third row). However, new texture components do not emerge during the annealing treatment. The texture develops faster at 473 K than at 373 K. Fig. 7 shows quantitative orientation data as acquired from a texture component fit in terms of the changes in the volume fraction and half width of the two main orientation components during the heat treatment. At 373 K the half width of the two orientation components decreases as a function of the annealing time. The volume fraction of the ⟨001⟩||RD fiber component remains almost constant while the {100}⟨001⟩ component slightly increases during heat treatment (Fig. 7a). This confirms a pronounced sharpening of the texture as qualitatively observed already from the pole figures. At 473 K the volume fraction of both texture components increases and their spherical half width decreases during annealing (Fig. 7b). The kinetics of texture sharpening are much faster at 473 K than at 373 K. The observed evolution of the texture happens at 473 K essentially within the first 10 min.

3.4. Evolution of crystallinity during heat treatment

The measurement of the change in crystallinity of the rolled PET during heat treatment is based on the integration of the background and Bragg-peak data over the entire pole sphere as already explained in Section 3.2 for the rolled samples.

Fig. 8a shows the integrated wide angle X-ray scans of a rolled PET sample (true rolling reduction $\phi=1.2$) as a function of time during isothermal heat treatment (373 K). Integration is conducted over all Debye–Scherrer frames measured for one sample condition. Fig. 8b shows the integrated number of all counts (full squares), the integrated number of background counts (full triangles), and the relative change in the number of all counts minus the background counts as a function of time during isothermal heat treatment. The latter curve (open squares) is a measure for the relative change in crystallinity during rolling.

Fig. 8a shows that the strong dominance of diffuse scatter which characterizes the integral scans after rolling (full squares) is rendered into a spectrum with less diffuse and increased Bragg diffraction upon heat treatment. This is quantified by Fig. 8b which substantiates a drop in the number of both, total and background counts, as well as an enhancement in the normalized fraction of all counts minus the background counts relative to all counts from ~4% to nearly ~12% (arbitrary units) indicating an increase in crystallinity.

Fig. 9 reveals the same analysis for 473 K. It can be observed that the increase in crystallinity is much faster and more pronounced than at 373 K. The integrated $\theta-2\theta$ scans reveal a very strong increase of the {100} Bragg diffraction peak (Fig. 9a) which is much less pronounced at 373 K. According to Fig. 9b the relative crystalline diffraction signal (open squares) at 473 K increases from ~4% to nearly ~27% (arbitrary units) after 40 min.

4. Discussion

4.1. Rolling texture

The rolling textures were calculated by use of the texture component method (Figs. 1–3). They are characterized by

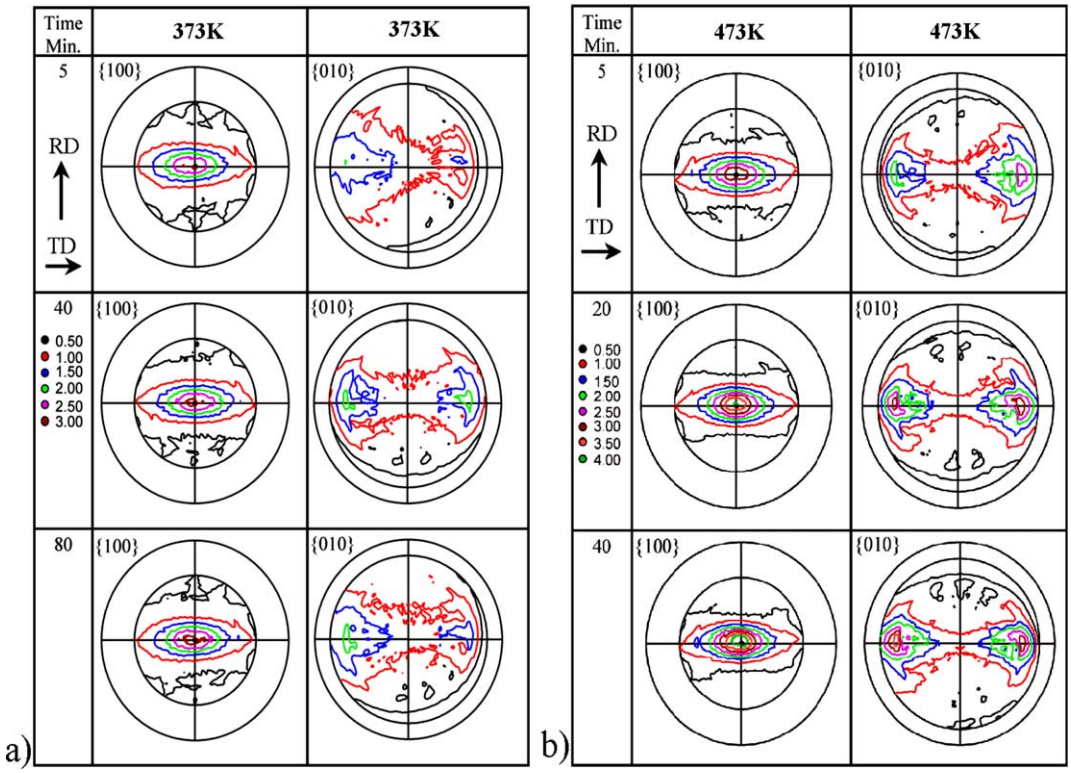

Fig. 6. Texture evolution in terms of pole figures of rolled ($\varphi = 1.2$) and subsequently heat treated PET. (a) 373 K (b) 473 K. When compared to the rolling textures shown in Fig. 1 the annealing textures are much sharper but not principally different.

the evolution of two main texture components, namely, a $\{100\}\langle 001\rangle$ component and a fiber component $\langle 001\rangle \| \mathrm{RD}$ (triclinic RD fiber component). Fig. 3 shows that the room temperature rolling texture, presented in terms of the volume fractions and spherical half widths of the two components, becomes stronger with increasing rolling strain. When the true strain exceeds a value of 1.2 the half widths become smaller indicating an increase in texture sharpness (less scatter of the texture components). The enhancement of texture sharpness upon rolling is an observation which is also frequently made for polycrystalline metals [24,25]. At a strain of 1.2 the $\{100\}\langle 001\rangle$ component is characterized by a relatively small volume fraction of only 4% and a large Gaussian scatter of 36.96° (full spherical width at half maximum). The triclinic RD fiber component occupies a volume fraction of 12.5% at a scatter of 23.2°.

A number of studies have tackled the relationship between the evolution of deformation textures in the crystalline parts of polymers and the underlying microscopic deformation mechanisms [1–6,14–16,26,27,32–39]. Excellent reviews on the underlying deformation mechanisms in semi-crystalline polymers were published by Bowden and Young [33], Haudin [34], Lotz and Wittmann [35], Crist [36] and by the group of Bartczak, Argon, and Cohen [14,27,37–39]. It was found in these works that the crystalline portions of HDPE, Nylon-6, and PET deform mainly by crystallographic shear mechanisms.

Although athermal mechanisms such as twinning and stress-induced martensite transformation were reported as well, they occurred only in highly textured samples, i.e. they are not assumed to act as main deformation mechanisms in the case of rolled samples as discussed in this work. According to these publications [33–39] it may be assumed that crystallographic slipping in the crystalline portions of semi-crystalline polymers occurs in the form of crystallographic shear predominantly on $\{hk0\}$ planes. This mechanisms is often referred to as crystallographic chain slip.

Although it seems not always clear from the literature whether such crystallographic chain slip occurs in the form of actual dislocation motion the crystallographic reorientations observed in this study clearly indicate Schmid-type behavior, i.e. the activation of an orientation dependent intralamellar shear mechanism. Instead of a direct dislocation motion and multiplication mechanism one might also argue that such crystallographic slip may in crystalline polymers occur in the form of simple rigid shears on van der Waals bonded (soft) planes or by the rigid intralamellar mutual shear of more compact small crystalline blocks within the same lamellae. The investigation of texture changes alone cannot resolve these fine nanoscopic differences though since they all entail the same plastic spin (provided they occur on the same crystalline planes and shear vectors). For instance, the relatively weak van der Waals bonding between neighboring covalently bonded

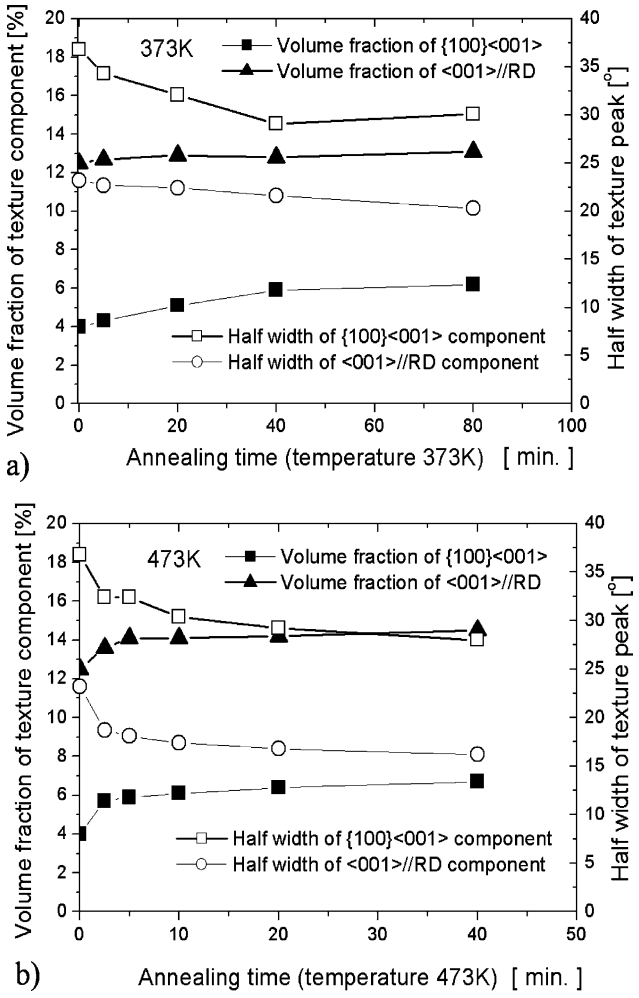

Fig. 7. Changes in the texture components during heat treatment. (a) 373 K, (b) 473 K.

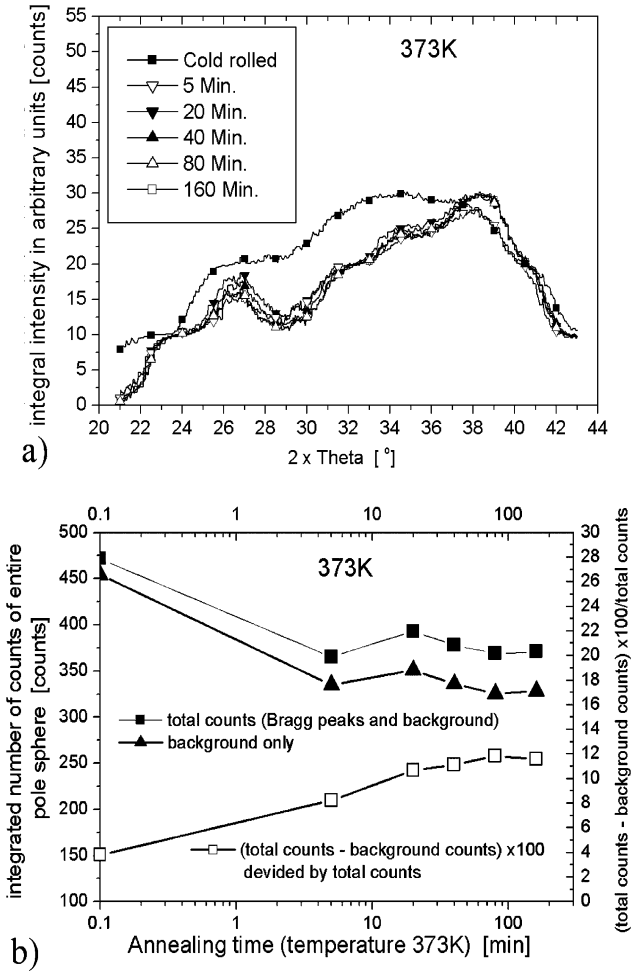

Fig. 8. (a) Integrated wide angle X-ray scans ($\theta-2\theta$ scans) of a rolled PET sample (rolling reduction $\varphi=1.2$) as a function of heat treatment time at a temperature of 373 K. Integration is conducted over all Debye–Scherrer frames measured for one sample condition. (b) Integrated number of all counts (full squares), integrated number of background counts (full triangles), and relative change (in %) in the number of all counts minus the background counts as a function of time during isothermal heat treatment. The latter curve (open squares) is a measure for the relative change in crystallinity during rolling.

molecule chains allows for glide between such chains in either the ⟨001⟩ chain axis direction or transverse direction ⟨uv0⟩. Such a soft mode of discrete crystallographic deformation may be assumed to require critical stresses of the order of the local shear modulus between such soft planes divided by ∼30. This means that crystallographic shear in PET does not necessarily require dislocation motion owing to the relatively weak bonds between the neighboring polymer segments which are lined up to form the crystals. A detailed discussion of these aspects is given in [36].

The literature in this field also shows that crystallographic slip in PET does not provide five independent shear systems [37–40] as required for a closed yield surface, owing to the low (triclinic) symmetry of the PET crystals. This means that the von Mises compatibility criterion is violated when considering crystallographic slip as the only mode of plastic deformation [41].

The most detailed experimental work on the interplay between crystallographic slip and the development of deformation textures in PET under plane strain conditions was conducted by Bellare et al. [6]. These authors reported that the initially spherulitic morphology was during deformation rendered into stacks of fragmented crystalline lamellae with lamellar normals oriented towards the flow direction. The authors suggested that that after some initial deformation by interlamellar sliding in the amorphous material (100) [001] crystallographic shear operated throughout the remainder of the deformation. Bellare et al. [6] assumed that this chain slip mechanism was responsible for the topological reorientation of the lamellar normals towards the compression axis. Further deformation caused fragmentation of the thinned-out lamellae and subsequent reorientation of lamellar normals towards the flow direction. From pole figure analysis the authors concluded that the cooperative activity of the (100)[001] chain slip and (100)[010] transverse slip was mainly responsible for the later stages of texture development. The (100)[010]

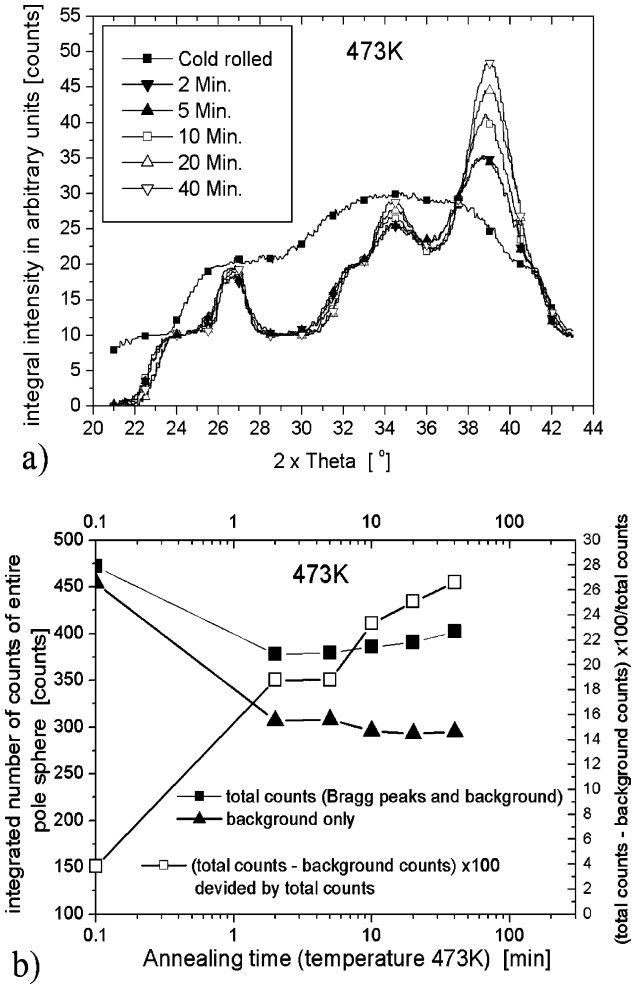

Fig. 9. (a) Integrated wide angle X-ray scans ($\theta-2\theta$ scans) of a rolled PET sample (rolling reduction $\varphi=1.2$) as a function of heat treatment time at a temperature of 473 K. Integration is conducted over all Debye–Scherrer frames measured for one sample condition. (b) Integrated number of all counts (full squares), integrated number of background counts (full triangles), and relative change (in %) in the number of all counts minus the background counts as a function of time during isothermal heat treatment. The latter curve (open squares) is a measure for the relative change in crystallinity during rolling.

transverse slip mechanism controlled the orientation of the crystal structure in a plane orthogonal to the flow direction. No evidence was found by the authors for the activity of (010)[001] chain slip. Since the (100)[001] chain slip system was the first observed crystalline deformation mechanism the authors concluded that it must have the lowest plastic resistance among the crystalline-phase deformation mechanisms. The slip resistance revealed a critical resolved shear stress of about 38 MPa.

Based on these experiments various groups have suggested models which describe the kinematics and micromechanics of deformation texture evolution in semi-crystalline polymers. The first micromechanical models for the simulation of the deformation and texture development in the crystalline portion of semi-crystalline polymers have been proposed by Lee et al. [14,15] and Ahzi et al. [32,40,42,43]. Proceeding from these investigations Van Dommelen and Parks et al. [16] suggested a more detailed deformation model which establishes links across the microscopic, mesoscopic, and macroscopic scales. An excellent overview is given in [32]. Concerning the simulation of texture evolution the authors report that their texture predictions match the data published previously by Bellare et al. [6].

We checked our experimental texture results with respect to the predominant crystallographic shear on (100)[001] as suggested by some of the articles mentioned above. For this purpose we used a simple Sachs model with three types of potential slip systems in order to obtain a qualitative understanding of the texture evolution. In accord with previous observations we find that the $\{100\}\langle001\rangle$ texture component (Figs. 1–3) can indeed be explained in terms of the activation of the $\{100\}\langle001\rangle$ slip system. The formation of the $\langle001\rangle\|$RD texture fiber, however, cannot be explained in terms of a simple Sachs approach. Since our observation confirms previous qualitative results obtained by pole figure analysis by Bellare et al. [6] we assume that the cooperative activity of the (100)[001] chain slip and (100)[010] transverse slip might be responsible for this type of smeared out fiber texture. One aspect which remains unclear in the current analysis is the rate dependence in the activation of the different slip systems.

4.2. Decrease in crystallinity during rolling

The gradual decrystallization observed during our room temperature rolling experiments is probably the most important observation of this study. Fig. 5 quantitatively shows the continuous strain-induced amorphization of the crystalline phase in the semi-crystalline PET as a function of the true plastic rolling strain. Fig. 5b shows the corresponding relative (normalized) change in the number of all X-ray counts minus the background signal as a function of deformation. The data show a drop in the relative diffraction signal with increasing total strain from ~15% to ~3%. This translates to a drop in the crystalline volume fraction from ~85% (undeformed) to ~17% at a true strain of 1.2. It must be noted that these data result from an integration of Bragg- and out-of-reflex counts over the entire pole sphere, i.e. the influence of the crystallographic texture is fully accounted for. The strain-induced amorphization of crystalline material in semi-crystalline polymers has also been referred to as *decrystallization* [36] or *disaggregation* [44–48].

A possible explanation of this gradual amorphization is that sheared crystalline lamellae break apart into sets of crystalline blocks which contain severe lattice defects [28–31,36]. This process is often referred to as mechanical melting. Such a mechanism would naturally entail substantial broadening of the Bragg cones before their total disappearance. This is indeed confirmed by our results as shown by the broad wide angle cones in Fig. 4. Our Debye–

Scherrer data show that there is no abrupt transition between the crystalline and the amorphous phase. The large Bragg broadening (which by far exceeds that observed for deformed metals) can be regarded as a kind of intermediate or semi-amorphous ordering state between the crystalline and the completely amorphous phase in accord with the model of a block-type arrangement of small crystalline portions with intermediate chain tangles.

Similar observations and related conclusions were during the last years published by the group of Strobl [44–48] on the basis of data obtained from uniaxial tensile testing. In these investigations the authors suggest that the process of tensile deformation consists of several regimes that are characterized by different types of deformation mechanisms. At small loads they assume that intralamellar slipping of crystalline blocks is the prevalent mechanism of deformation. At larger strains above the yield strain they observe a stress-induced crystalline block disaggregation–recrystallization process. In a recent work Men et al. [44] suggested that the strain at this transition point between the two regimes is related to the interplay between the amorphous entanglement density and the mechanical stability of the crystal blocks. The authors furnished this two-stage deformation model by careful experimental evidence obtained from true stress–strain curves. The authors also concluded in this article that tie molecules, which connect adjacent lamellae, were assumed to be of lesser importance with respect to such type of deformation behavior.

Apart form these basic and largely consistent observations of the strain-induced drop in crystallinity (disaggregation–recrystallization process) our measurements also show the evolution of pronounced deformation textures (Figs. 1–3). This means that the strain-induced amorphization observed must not be regarded as a texture-independent process. In order to reconcile these two observations (*disaggregation–recrystallization* of crystals versus *reorientation* of crystals) we suggest that in particular those crystalline lamellae which cannot deform by crystallographic (100) [001] chain or respectively inter-block shear, due to their vanishing Schmid factor, are prone to undergo transition into the amorphous phase. In simple terms this means that the evolution of crystallographic texture and the strain-induced amorphization of crystals are linked via the orientation factor of the crystalline material. Of course this effect is governed by the local and not be the global mechanical boundary conditions as discussed in the introduction.

This argumentation suggests that deformation-induced amorphization must be regarded as a natural microscopic deformation mode in semi-crystalline PET. In particular it can be regarded as an isotropic rather than a anisotropic crystallographic contribution to the yield locus. This is schematically presented in Fig. 10. Our concept assumes that the easiest mode of deformation for a crystalline lamella is the shear on a (100)[001] chain or respectively inter-block slip system. When stressed along a direction, which does not favor activation of this system, the respective crystal undergoes amorphization as an alternative mode of deformation. In other words if the local stress in a PET crystal reaches the yield surface in any direction other than that prescribed by single slip the lamella is decrystallized, i.e. it starts to disintegrate as a compatible mode of deformation. Since Figs. 1 and 2 as well as a number of previous authors clearly substantiate the evolution of deformation textures on the basis of chain slip it may be concluded that the critical stress for the activation of strain-induced amorphization is larger than that for the activation of (100)[001] chain slip. Since the background analysis reveals that crystallinity continuously drops during rolling according to the gradual formation of a pronounced (100)[001] texture component we suggest that amorphization acts in the present case as an alternative deformation mechanism to further crystallographic slip particularly in crystals with (100)[001] orientation.

Although this picture is fully consistent with previous suggestions on the gradual sequence of intralamellar slipping of crystalline blocks as dominant mechanism at small strains and a stress-induced crystalline block disaggregation–recrystallization process at larger strains [44–48] it adds one more important aspect to this model. This further detail is the suggestion that both mechanisms may even occur at the same strain level, however, differently in different crystalline lamellae, according to their respective crystalline orientation factors. This means that while some crystals start to disintegrate already at rather small strains according to their unfavorable Schmid factors, others may (at least in part) remain mechanically stable also up to higher strains, but they reorient according to the plastic spin resulting from their respective active slip or block shear system. The evidence for this assumption comes directly from two facts. First, not all of the formerly crystalline volume is rendered amorphous upon deformation. Second, the crystalline volume which gradually decreases during rolling develops a pronounced texture which can be explained in terms of characteristic crystallographic intralamellar shear systems.

4.3. Evolution of crystallographic texture and crystallinity during heat treatment

Heat treatment (373, 473 K) of the sample rolled to a true strain of 1.2 leads first, to the recrystallization of amorphous material and second, to an enhancement of the original deformation texture. This applies in particular to the samples which were heat treated at 473 K. Fig. 9 shows a strong change of the relative diffraction signal as a function of time during the isothermal heat treatment. Figs. 6 and 7 show that this strong recrystallization process does obviously not lead to new crystalline orientations, but merely to a sharpening of the preceding rolling texture (see Figs. 1–3). This leads us to the conclusion that

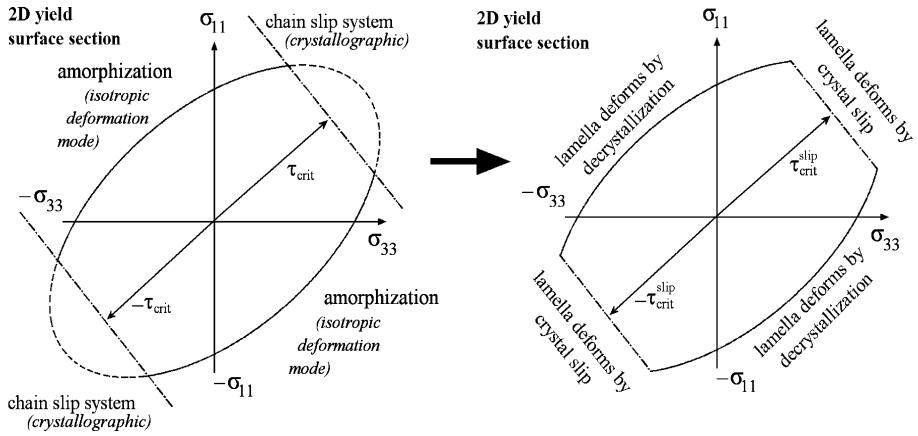

Fig. 10. Schematical figure of a 2D section through a 5D yield surface of a crystalline lamella in semi-crystalline PET. We suggest amorphization (decrystallization) as an orientation-dependent deformation mechanism. It can be regarded as an isotropic rather than an anisotropic, crystallographic contribution to the yield locus. Our concept assumes that the easiest mode of deformation for a crystalline lamella is the shear on a (100)[001] chain slip system. When stressed along a direction which does not favor activation of this system, the crystal is assumed to undergo amorphization.

recrystallization works in the present case by an oriented nucleation or, respectively, relaxation mechanism where the amorphous material aligns along existing crystalline lamellae or fragmented lamellae blocks which were not decrystallized during rolling. By relaxation we mean that it is conceivable that the observed recrystallization process might occur via the re-alignment of the small crystalline blocks which were suggested as a typical microstructure of rolled and broken lamellae. This argumentation is supported by the strong sharpening of the Bragg cones (Fig. 9a) upon heat treatment.

5. Conclusions

We conducted a quantitative experimental study on crystallographic texture, amorphization (decrystallization), and recrystallization in rolled and heat treated polyethylene therephthalate (PET). The main conclusions are:

- Quantitative texture analysis (texture component method) revealed a strong $\{100\}\langle001\rangle$ texture component and an incomplete texture fiber with a $\langle001\rangle$ axis‖rolling direction after room temperature rolling. The texture was attributed to crystallographic shear mainly on the $\{100\}\langle001\rangle$ system. The observations are in excellent accordance with earlier experimental findings as well as with texture simulations reported in the literature.
- It was observed that crystallinity continuously drops during rolling from ∼85% (undeformed) to ∼17% at a true strain of 1.2 (decrystallization, amorphization). We suggested that amorphization can be regarded as a deformation mechanism which may take place as an alternative to crystallographic slip depending on the crystal orientation of a lamella. We suggested a yield surface which accounts for both, decrystallization and crystallographic slip as partially competing deformation mechanisms.
- We observed large broadening of the Bragg cones during deformation which we discussed in terms of a gradual strain-induced transition from the crystalline to the amorphous phase.
- Heat treatment (373, 473 K) of rolled samples leads to the recrystallization of amorphous material and to an enhancement of the original deformation texture. This observation was explained in terms of an oriented nucleation or respectively relaxation mechanisms where amorphous material aligns along existing crystalline lamellae or fragmented lamellae blocks.

References

[1] Llana PG, Boyce MC. Polymer 1999;40:6729.
[2] Asano T, Balta Calleja FJ, Flores A, Tanigaki M, Mina MF, Sawatari C, Itagaki H, Takahashi H, Hatta I. Polymer 1999;40:6475.
[3] Asano T, Yamamoto T, Mina MF, Fujiwara Y, Takahashi H, Hatta I. J Macromol Sci Phys 1999;B38:163.
[4] Mahendrasingama A, Blundell DJ, Martin C, Fuller W, MacKerron DH, Harviec JL, Oldman RJ, Riekeld C. Polymer 2000; 41:7803.
[5] Bedia EL, Murakami S, Kitade T, Kobjiya S. Polymer 2001;42:7299.
[6] Bellare A, Cohen RE, Argon AS. Polymer 1993;34:1393.
[7] Goschel U, Deutscher K, Abetz V. Polymer 1996;37:1.
[8] Mahendrasingama A, Martin C, Jaber A, Hughes D, Fuller W, Rule R, Oldman RJ, Blundell DJ, MacKerron DH. . Nuclear Instr Meth Phys Res 1995;97B:238.
[9] Blundell DJ, Mahendrasingama A, Martin C, Fuller W, MacKerron DH, Harvie JL, Oldmapoan RJ, Riekel C. Polymer 2000;41:7793.
[10] Bunge HJ. Texture analysis in materials science. London, England: Butterworths; 1982.
[11] Raabe D, Lücke K. Phys Status Solidi (B) 1993;180:59.
[12] Barham PJ. Polymer 1982;23:1112.
[13] Barham PJ, In: Thomas EL (ed.) Structure and properties of polymers, vol. 12; Cahn RW, Haasen P, Kramer EJ (Series Ed.) Materials science and technology, p. 153; 1993.

[14] Lee BJ, Argon AS, Parks DM, Ahzi S, Bartczak Z. Polymer 1993;34:3555.
[15] Lee BJ, Parks DM, Ahzi S. J Mech Phys Solids 1993;41:1651.
[16] Nikolov S, Doghri I, Pierard O, Zealouk L, Goldberg A. J Mech Phys Solids 2003;50:2275.
[17] Van Dommelen JAW, Parks DM, Boyce MC, Brekelmans WAM, Baaijens FPT. Polymer 2003;44:6089.
[18] Chaari F, Chaouche M, Doucet J. Polymer 2003;44:473.
[19] Gorlier E, Haudin JM, Billon N. Polymer 2001;42:9541.
[20] Zhang Z, Ren M, Zhao J, Wu S, Sun H. Polymer 2003;44:2547.
[21] Lücke K, Pospiech J, Virnich KH, Jura J. Acta Metall 1981;29:167.
[22] Helming K, Schwarzer RA, Rauschenbach B, Geier S, Leiss B, Wenk HR, Ullemeier K, Heinitz J. Z Metallkunde 1994;85:545.
[23] Encyclopedia of polymer science and engineering, 2nd ed. New York: Wiley; 1985.
[24] Hölscher M, Raabe D, Lücke K. Steel Res 1991;62:567.
[25] Raabe D, Lücke K. Mater Sci Technol 1993;9:302.
[26] Nikolov S, Doghri I. Polymer 2000;41:1883.
[27] Bartczak Z, Argon AS, Cohen RE. Polymer 1994;35:3427.
[28] Gupta VB, Kumar S. Polymer 1978;19:953.
[29] Eichhoff U, Zachmann HG. Makromol Chem 1971;(147):41.
[30] Wu J, Schultz JM. Polymer 2002;43:6695.
[31] Ajji A, Guevremont J, Cole KC, Dumulin MM. Polymer 1996;37:3707.
[32] Ahzi S, Lee BJ, Asaro RJ. Mater Sci Eng A 1994;189:35.
[33] Bowden PB, Young RJ. J Mater Sci 1974;9:2034.
[34] Haudin JM. Plastic defor-mation of amorphous and semi-crystalline materials. In: Escaig B, G'Sell C, editors.. Les Ulis: Les Editions de Physique; 1982. p. 291.
[35] Lotz B, Wittmann J-C, In: Thomas EL (ed.) Structure and properties of polymers, vol. 12; Cahn RW, Haasen P, Kramer EJ (Series ed.) Materials science and technology, p. 79; 1993.
[36] Crist B, In: Thomas EL (ed.) Structure and properties of polymers, vol. 12; Cahn RW, Haasen P, Kramer EJ (Series ed.) Materials science and technology, p. 427; 1993.
[37] Bartczak Z, Argon AS, Cohen RE. Macromolecules 1992;25:5036.
[38] Lin L, Argon AS. Macromolecules 1992;25:4011.
[39] Bellare A, Cohen RE, Argon AS. Polymer 1993;34:1393.
[40] Ahzi S, Parks DM, Argon AS. In: Singh B, Im YT, Haque I, Allan C, editors. Computer modeling and simulation of manufacturing processes. New York: ASME; 1990. p. 287.
[41] Raabe D, Klose P, Engl B, Imlau KP, Friedel F, Roters F:. Adv Eng Mater 2002;4:169.
[42] Parks DM, Ahzi S. In: Dvorak GJ, editor. IUTAM symposium on inelastic behavior of composite materials. New York: Springer; 1990. p. 325.
[43] Parks DM, Ahzi S. J Mech Phys Solids 1990;38:701.
[44] Men YF, Rieger J, Strobl G. Phys Rev Lett 2003;91:095502.
[45] Hiss R, Hobeika S, Lynn C, Strobl G. Macromolecules 1999;32:4390.
[46] Hobeika S, Men Y, Strobl G. Macromolecules 2000;33:1827.
[47] Men YF, Strobl G. J Macromol Sci Phys B 2001;40:775.
[48] Men YF, Strobl G. Macromolecules 2003;36:1889.